Tetrahedron xxx (2015) 1–12

Contents lists available at ScienceDirect

Tetrahedron

journal homepage: www.elsevier.com/locate/tet

Synthesis and fluorescence properties of 4-diarylmethylene analogues of the green fluorescent protein chromophore

Masahiro Ikejiri [a], Kousuke Matsumoto [a], Hiraku Hasegawa [a], Daisuke Yamaguchi [a], Moe Tsuchino [a], Yoshiko Chihara [a], Takao Yamaguchi [b], Kazuto Mori [b], Takeshi Imanishi [b], Satoshi Obika [b], Kazuyuki Miyashita [a,*]

[a] Faculty of Pharmacy, Osaka Ohtani University, Nishikiori-Kita 3-11-1, Tondabayashi, Osaka 584-8540, Japan
[b] Graduate School of Pharmaceutical Sciences, Osaka University, Yamadaoka 1-6, Suita, Osaka 565-0871, Japan

ARTICLE INFO

Article history:
Received 15 April 2015
Received in revised form 20 May 2015
Accepted 21 May 2015
Available online xxx

Keywords:
Fluorescence
Chromophore
Imidazolinones
Green fluorescent protein

ABSTRACT

New green fluorescent protein (GFP) chromophore analogues, namely 4-(diarylmethylene)imidazolinones (DAINs), were readily synthesized under weakly acidic conditions using a novel condensation reaction between methyl imidate (or thioimidate) and ethyl *N*-(diarylmethylene)glycinate. DAINs showed notable fluorescence properties. Although they were nearly non-fluorescent in the solution, visible emissions were detected in most of their frozen solution states and crystalline powder states. Therefore, control of the molecular motions significantly affected emissions by DAINs. Comparison of the fluorescence properties of DAIN **5a** with those of the corresponding GFP-chromophore analogues **8** revealed that **5a** possessed superior solid-state fluorescence properties.

1. Introduction

Green fluorescent protein (GFP) is a well-known fluorescent protein, and is widely employed as a useful imaging tool because it can help visualise various biological events through highly sensitive fluorescence detection.[1] The chromophore within GFP is formed from a Ser-Tyr-Gly tripeptide in the primary protein structure by post-translational cyclodehydration and subsequent oxidation to yield the 4-(*p*-hydroxybenzylidene)imidazolinone (HO-BDI) moiety. The conformation of the HO-BDI chromophore is restricted to the *Z*-form within the GFP β-barrel tertiary structure, which enables emission by GFP.[2] However, outside the protein, fluorescence quenching of the chromophore is induced mainly by molecular motions such as the free rotation of the aryl–alkene single bond and the double bond isomerization of the *Z*-4-hydroxybenzylidene moiety ('bright' form) to the corresponding *E*-isomer,[3,4] which is generally known to exhibit extremely weak fluorescence ('dark' form),[5] although exceptions are known[6] (Fig. 1A).

In an effort to prepare new small-molecule fluorescent materials, we designed a series of diarylmethylene-based compounds, namely 4-(diarylmethylene)imidazolinones (DAINs), as novel analogues of the GFP chromophore (Fig. 1B). Our design comprised three

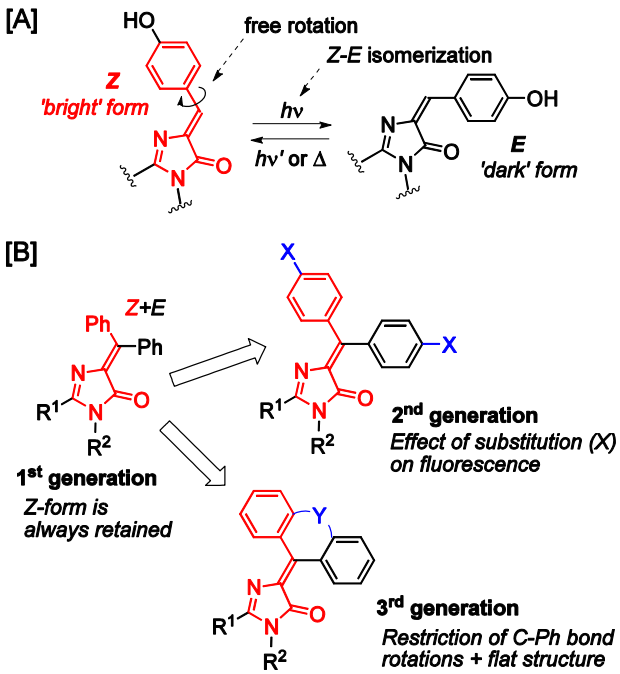

Fig. 1. A. Structure of the GFP chromophore (HO-BDI). B. Design of the model compound, 4-(diarylmethylene)imidazolinone (DAIN).

* Corresponding author. Tel.: +81 721 24 9652; fax: +81 721 24 9652; e-mail address: miyasik@osaka-ohtani.ac.jp (K. Miyashita).

http://dx.doi.org/10.1016/j.tet.2015.05.073
0040-4020/

structural generations. The first generation contained a diphenylmethylene unit on the imidazolinone ring. Because this moiety is symmetrical, the structure is the same after the double-bond isomerization. Therefore, the fluorescence (attributed to the *Z*-form) could be maintained regardless of the isomerization. The second- and third-generation structures were designed by focusing on the diarylmethylene moiety. As a common imidazolinone moiety of these two generations, we selected a 1,2-pentanoimidazolinone structure based on the fluorescence properties of the first-generation DAINs **1**–**7** (Fig. 2), whose details are described in Section 2.2.1.1. The second-generation structures were designed to elucidate substituent effects (electron donating and electron withdrawing) on the diphenyl moiety of the first-generation compounds (DAINs **5b** and **5c**). In the third generation, the diphenyl rings were designed to be in nearly the same plane as the imidazolinone ring by installing a bridge between the diphenyl rings (DAINs **5d** and **5e**). Such installation would prevent C–Ph free rotation. We expected that this third generation would exhibit the strongest emission because of the overall structural advantages described above. Although several types of 4-benzylideneimidazolinone (BDI) analogues with substantial fluorescence have been reported so far,[7–10] to the best of our knowledge, there has been no report on such diarylmethylene analogues of the GFP chromophore. In this study, we report the synthesis of the DAIN series (Section 2.1) and their fluorescence properties, including a comparison of DAIN **5a** with analogous BDI compounds, *Z*- and *E*-**8** (Section 2.2).[11]

2. Results and discussion

2.1. Synthesis of the DAIN series

2.1.1. Optimization of reaction conditions. Although several synthetic approaches towards BDI-based structures have been reported,[10,12,13] no effective approaches towards DAIN structures are known. Notably, the syntheses used for BDI[10,12] were ineffective in the synthesis of DAIN **1**. Thus, we endeavoured to develop a novel synthetic method to obtain DAIN **1**, and eventually identified a suitable concise condensation reaction between methyl thioimidate **9a** and ethyl *N*-(diphenylmethylene)glycinate **10a**, as shown in Table 1. Although the product, **1**, was not yielded by mixing **9a** and **10a** at room temperature, it was obtained in 52%–60% yield in hot solvents like toluene and 1,2-dichloroethane, although a long reaction time was required (Table 1, runs 1–4). However, contrary to our expectations, the product was not

Table 1
Reaction of thioimidate **9a** with *N*-(diphenylmethylene)glycinates **10a**–**d**

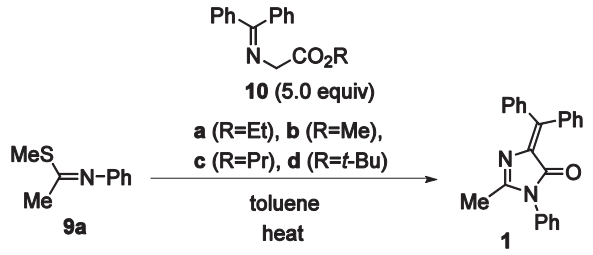

Run	**10**	Temp (°C)	Additive [equiv]	Time (days)	Yield (%)
1	**a**	rt	None	7.0	0
2	**a**	70	None	7.0	55
3	**a**	80	None	4.0	60
4	**a**	80	None	3.0	52[a]
5	**a**	Reflux	None	7.0	Trace[b]
6	**a**	80	EtOH [5.0]	2.5	43
7	**a**	80	BuSH [1.0]	3.0	58
8	**a**	80	AcOH [1.0]	1.0	64
9	**a**	Reflux	AcOH [2.0]	1.0	78
10	**a**	rt to reflux	MsOH [2.0]	1.0	0[c]
11	**a**	Reflux	$ZnCl_2$ [2.0]	0.1	0[c]
12	**a**	Reflux	LiCl [2.0]	1.0	0[b]
13	**b**	Reflux	AcOH [2.0]	1.0	7[d]
14	**c**	Reflux	AcOH [2.0]	1.0	12[d]
15	**d**	Reflux	AcOH [2.0]	1.0	13[d]

[a] $ClCH_2CH_2Cl$ was used as the solvent.
[b] Almost no reaction.
[c] Complex mixture.
[d] The reaction was not complete within 24 h.

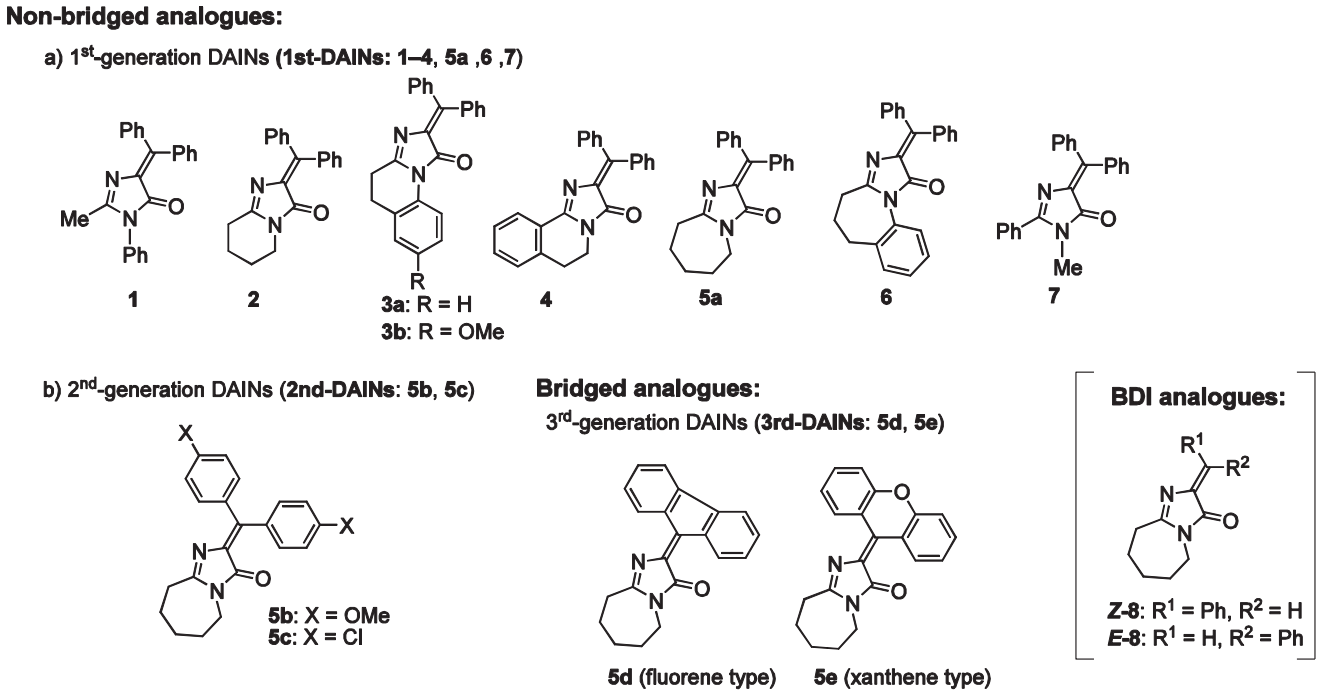

Fig. 2. Structures of DAIN series and BDI analogues.

obtained under reflux in toluene (run 5). As this result appeared to suggest an important role of the volatile methanethiol and/or ethanol produced during the course of the reaction, the reaction was conducted in the presence of a mild protic additive (runs 6–9). The addition of protic additives shortened the reaction time, and acetic acid in refluxing toluene produced the best result (run 9). The use of a stronger protic acid (methanesulfonic acid) or Lewis acids such as $ZnCl_2$ and LiCl were ineffective (runs 10–12). Surprisingly, the identity of the alkyl group on the ester moiety of **10** significantly influenced the reaction. The use of an ethyl group afforded a promising result, whereas the use of other moieties such as methyl, propyl and *tert*-butyl groups resulted in a slow reaction (run 9 vs runs 13–15). Thus, this reaction seemed to be affected by the steric hindrance and electron donation ability of the alkyl group.

2.1.2. Synthesis of 1st-generation DAINs. To obtain the first-generation DAINs, various thioimidates and imidates, shown in Fig. 3, were used as the starting materials; the results are summarised in Table 2. The products of the reactions with most thioimidates were obtained in good to moderate yields (Table 2, runs 1–7). An increased amount of acetic acid was effective in the case of slow reaction (run 3 vs 4). Interestingly, the use of imidates was effective (runs 8–10, and 14), and afforded better results than those of the corresponding thioimidates in regard to the yields and reaction times (run 1 vs 8; 2 vs 9; 6 vs 10), even though the imidates were less stable than the thioimidates. The reaction could even be conducted at room temperature using aliphatic imidates such as **9b-*O*** and **9f-*O***, although a longer reaction time was required (runs 15 and 16). A decreased amount of **10a**, the use of **10b**, and AcOH-free conditions resulted in poor yields even when imidate **9f-*O*** was used (run 10 vs runs 11–13). Unfortunately, aromatic imidate and thioimidate **9i** were not viable substrates in this reaction (runs 17 and 18).

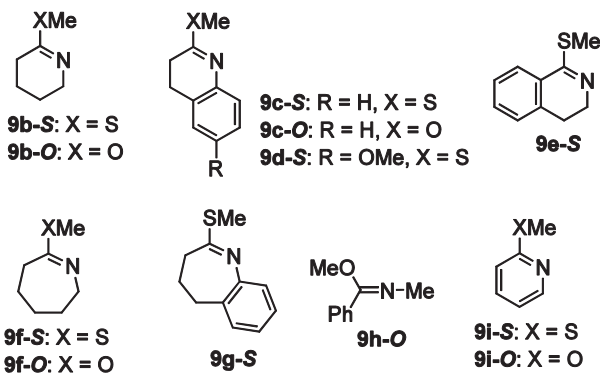

Fig. 3. Structures of thoimidates and imidates **9b**–**i**.

2.1.3. Synthesis of 2nd- and 3rd-generation DAINs. To obtain the second- and third-generation DAINs, coupling reactions with imidate **9f-*O*** and several glycinates with a particular diarylmethylene moiety, as shown in Fig. 4,[14] were respectively conducted, and the results are summarized in Table 3.

All reactions proceeded smoothly even at room temperature (runs 1–4); notably, bridged type *N*-(diarylmethylene)glycinates **10g** and **10h** reacted despite the use of fewer equivalents (3.0 equiv, runs 3 and 4). The substituent on the benzene ring of the diphenyl moiety affected the reaction yield; an electron-donating group (–OMe, **10e**) gave a higher yield (70%), whereas an electron-withdrawing group (–Cl, **10f**) resulted in a lower yield (52%) as compare to no substituent (–H, **10a**, 60%) (runs 1 and 2 vs Table 2, run 16). Therefore, the stability of the benzylic carbocation at the diarylmethylene moiety seemed to affect the reactivity. Notably, at reflux, the substituents did not seem to have a noticeable effect (runs 5 and 6 vs Table 2, run 10) probably due to the instability of the product at high temperatures; for instance, prolonged treatment of **10e** and **10f** under reflux for 18 h resulted in a marked

Table 2
Reaction of (thio)imidates **9b**–**i** with *N*-(diphenylmethylene)glycinate **10a**

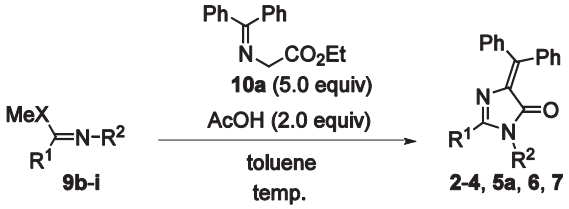

Run	9	Temp	Time (hours)	DAIN	Yield (%)
1	**b-*S***	Reflux	24	**2**	43
2	**c-*S***	Reflux	36	**3a**	77
3	**d-*S***	Reflux	36	**3b**	42
4	**d-*S***	Reflux	24	**3b**	75[a]
5	**e-*S***	Reflux	36	**4**	68
6	**f-*S***	Reflux	48	**5a**	27
7	**g-*S***	Reflux	36	**6**	89
8	**b-*O***	Reflux	5	**2**	71
9	**c-*O***	Reflux	24	**3a**	85
10	**f-*O***	Reflux	4	**5a**	59
11	**f-*O***	Reflux	6	**5a**	29[b]
12	**f-*O***	Reflux	24	**5a**	25[c]
13	**f-*O***	Reflux	4	**5a**	5[d]
14	**h-*O***	Reflux	20	**7**	77
15	**b-*O***	rt	96	**2**	32
16	**f-*O***	rt	24	**5a**	60
17	**i-*S***	Reflux	24	—	0
18	**i-*O***	Reflux	24	—	0

[a] 4.0 equiv of AcOH was used.
[b] 3.0 equiv of **10a** was used.
[c] 5.0 equiv of **10b** was used.
[d] Without AcOH (reaction did not go to completion).

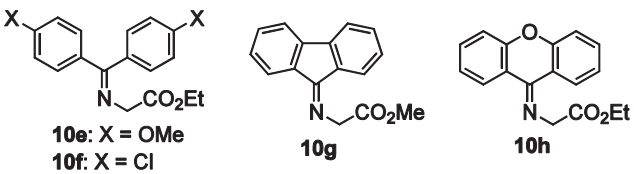

Fig. 4. Structures of *N*-(diarylmethylene)glycinates **10e**–**h**.

Table 3
Reaction of imidate **9f-*O*** with *N*-(diarylmethylene)glycinates **10e**–**h**

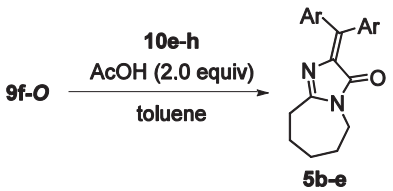

Run	10 [equiv]	Conditions	5	Yield (%)
1	**e** [5.0]	rt, 24h	**b**	70
2	**f** [5.0]	rt, 34h	**c**	52
3	**g** [3.0]	rt, 24h	**d**	85
4	**h** [3.0]	rt, 24h	**e**	74
5	**e** [5.0]	Reflux, 4h	**b**	42
6	**f** [5.0]	Reflux, 8h	**c**	15
7	**e** [5.0]	Reflux, 18h	**b**	28
8	**f** [5.0]	Reflux, 18h	**c**	9

decrease in the product yields (runs 7 and 8), as opposed to that of **10a** (reflux, 18h, 51% yield of **5a**).

2.1.4. Reaction mechanism. A possible reaction mechanism for the DAIN synthesis is depicted in Fig. 5. A notable feature of this reaction is that the diarylmethylene moiety migrates from the nitrogen to the α-carbon. Specifically, an attack of the imine-nitrogen, and not the α-carbanion of **10**, on the (thio)imidate **9** appears to be the first step of this reaction to form iminium intermediate **A**. In this step, the addition of a proton source would aid in the activation of the (thio)imidate-nitrogen. Subsequently, following the enolation and transformation into carbocation intermediate **B**, an intramolecular aziridine formation would occur to afford **C** and then **D**. Concomitant aziridine-ring cleavage of **D** promoted by α-deprotonation would produce the DAIN structure, accompanied by the migration of the diarylmethylene moiety from the nitrogen to the α-carbon. Although we could not isolate the aziridine intermediate, Ayyangar and co-workers reported an aziridine synthesis from glycinate **10a**.[15]

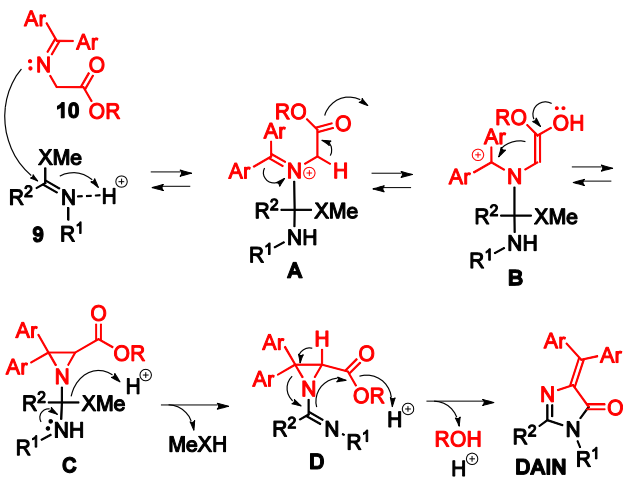

Fig. 5. A possible reaction mechanism for the DAIN synthesis.

The different reactivities of *N*-(diarylmethylene)glycinates **10a**–**h** could be explained if the reaction occurred via the aforementioned pathway. The reactivity derived from the diarylmethylene moiety would be related to the carbocation formation step (**A** to **B**), since a stable carbocation seemed to accelerate the reaction as shown in Table 3. The choice of the ester alkyl group (Table 1 runs 9, 13–15), would affect the aziridine formation (**B** to **C**) and the final cyclization (**D** to **DAIN**). The aziridine formation would be facilitated by the electron donation of the ester alkoxy group, but this step and the final cyclization step would be interrupted by the steric hindrance of the ester alkyl group due to the crowded reaction space. The ethyl group could be of a suitable size to meet these factors (high electron donation and small size). Additionally, the electron donation of the diaryl moiety with methoxy substitutions and that of the ester alkyl group would also accelerate the first addition step of **10** to **9**.

2.1.5. Analysis of the DAIN structure. The structures of the DAIN analogues were confirmed with ^{1}H NMR, ^{13}C NMR, mass spectrometry, and elemental analysis. In addition, for representative samples (i.e., **1**, **3a**, **5d** and **6**), the structure was confirmed with X-ray crystal structural analysis, whose details are described in Section 2.2.2.2. IR and UV–vis absorptions were also helpful in elucidating the DAIN structures, due to characteristic absorptions (Table 4). In the case of diphenylmethylene-containing species, two strong absorptions were detected in the IR spectra around 1615–1640 cm^{-1} and 1700–1715 cm^{-1}, probably owing to the two carbon-heteroatom double bonds in the imidazolinone ring; in addition, an absorption was detected around 360–400 nm in the UV–vis spectra, which was attributed to the DAIN ring system (runs 1–8). Modification of the diphenyl moiety shifted the absorptions slightly; the wavenumber of the IR absorption tended to decrease except for one absorption of **5c** (1705 cm^{-1}), while the UV–vis absorption was red-shifted (runs 6 vs 9–12).

Table 4
Characteristic IR and UV–vis absorption of DAIN series

Run	DAIN	IR (cm^{-1})[a]	UV–vis (nm)[b]
1	**1**	1620, 1715	357
2	**2**	1619, 1703	365
3	**3a**	1634, 1710	370
4	**3b**	1637, 1708	390[c]
5	**4**	1620, 1706	397
6	**5a**	1623, 1700	362
7	**6**	1625, 1712	367
8	**7**	1616, 1707	390
9	**5b**	1601, 1696	384
10	**5c**	1619, 1705	370
11	**5d**	1601, 1696[d]	406
12	**5e**	1605, 1688	412

[a] Representative wavenumbers around 1600–1720 cm^{-1} (diffuse reflection in KBr).
[b] λ_{max} of the longest wavelength absorption (1.0×10^{-5} M in CH_2Cl_2).
[c] Detected as a shoulder peak around 360–420 nm.
[d] Another absorption was detected at 1626 cm^{-1} (medium).

*2.1.6. Synthesis of BDI analogues **8**.* BDI analogues **8**, which are analogous to **5a**, were synthesised for comparison, as shown in Scheme 1. Initially, we attempted to apply the synthetic method of DAINs to the synthesis of BDIs by using imidate ***9f-O*** and glycinate **11** instead of **10a**. However, the desired product ***Z*-8** was not obtained. Because a convenient BDI synthesis based on the aza-Wittig reaction has been reported,[10] we adopted the reported method as an alternative route. Lactam **12** was transformed into azidoacetyl derivative **14** through chloroacetyl intermediate **13** in 33% yield over two steps. The aza-Wittig reaction of **14** was performed by treatment with Ph_3P to afford imidazolinone **15** in 90% yield. Because the total yield of these three steps was moderate (30%), we also adopted a modified version of Campagna's procedure[16] using glycine methyl ester hydrochloride, by which **15** was easily obtained from imidate ***9f-O*** in good yield (96%). Finally, imidazolinone **15** was coupled with benzaldehyde in the presence of piperidine to afford BDI ***Z*-8** exclusively in 70% yield. The *Z*-benzylidene moiety in ***Z*-8** was isomerised under UV light to form the *E*-isomer ***E*-8** in 43% yield, as with other reported BDI analogues.[3,5] The *E*-isomer was reisomerised to ***Z*-8** under UV or visible light. The *Z*-, *E*-geometry of **8** was determined by comparison of the ^{1}H NMR chemical shifts of the olefin hydrogen to those of structurally similar known compounds.[5]

2.2. Fluorescence evaluation

2.2.1. Results

2.2.1.1. Fluorescence properties of 1st-generation DAINs. Initially, we examined the fluorescence properties of the first-generation DAINs **1**–**4**, **5a**, **6** and **7** (**1st-DAINs**) in CH_2Cl_2, benzene and dimethyl sulfoxide (DMSO); however, all the compounds were nearly

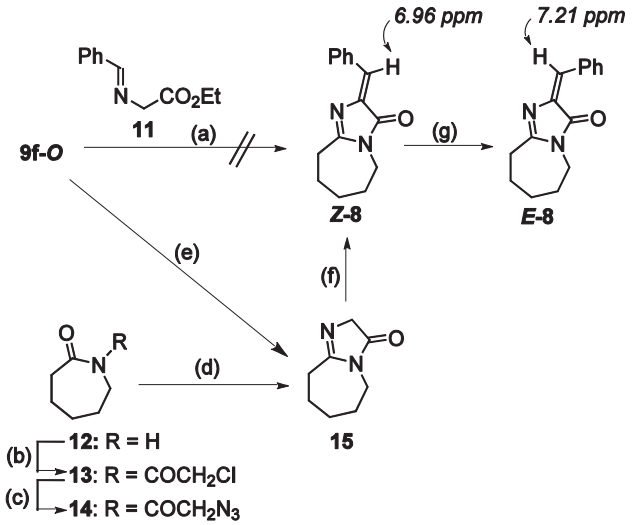

Scheme 1. Synthesis of BDIs **8**. Reagents and conditions: (a) **11**, AcOH, toluene, reflux; (b) $ClCH_2COCl$, Et_3N, CH_2Cl_2, rt; (c) NaN_3, DMSO, rt, 33% from **12**; (d) Ph_3P, toluene, rt, 90%; (e) $HCl{\cdot}H_2NCH_2CO_2Me$, Et_3N, MeOH, reflux, 96% (f) PhCHO, piperidine, MeOH, rt, 70% (g) 365 nm UV, benzene, rt, 43% (recovery of ***Z*-8**, 42%).

non-fluorescent in the solution state, contrary to our expectations. In contrast, a number of analogues exhibited emission visible to the naked eye in the crystalline powder state,[17] with the exception of **1**. Real-colour photographs of the fluorescence of crystalline powders of **1st-DAINs** are shown in Fig. 6 (black numbers correspond to **1st-DAINs**). Emissions ranging in colour from cyan to yellow were visually observed. The fluorescence profiles of crystalline powder **1st-DAINs** are listed in Table 5 (runs 1–8), and excitation and emission spectra of representative compounds are given in Fig. 7. As an approximate estimation of the fluorescence intensity, the relative intensity (R.I.) of each analogue was calculated from the integral of the emission spectrum to that of standard compound **5a**, and regarding representative analogues, their quantum yields (Φ) were also measured. The excitation wavelengths (λ_{ex}) were detected at approximately 370 nm for most compounds, although it was difficult to assign accurate values because of the broadness of the spectra. In contrast, the emission wavelengths (λ_{em}) were detected

Table 5
Fluorescence of DAINs **1**–**7** in the crystalline powder state

Run	DAIN	Gen.	λ_{ex}	λ_{em}	R.I.[a]
1	**1**	1st	370	506	0.03
2	**2**	1st	369	504	0.17
3[g]	**3a**	1st	369	531	0.72[b]
4[g]	**3b**	1st	370	540	0.81
5	**4**	1st	367	505	1.13[c]
6	**5a**	1st	370	513	1.00[d]
7	**6**	1st	371	493	2.20[e]
8	**7**	1st	369	535	0.31
9	**5b**	2nd	370	517	0.50[f]
10	**5c**	2nd	371	486	0.06
11	**5d**	3rd	403	566	<0.01
12	**5e**	3rd	491	563	0.01

[a] Emission intensity relative to that of **5a**.
[b] $\Phi_{\mathbf{3a}}$: 9.8%.
[c] $\Phi_{\mathbf{4}}$: 19.4%.
[d] $\Phi_{\mathbf{5a}}$: 16.3%.
[e] $\Phi_{\mathbf{6}}$: 33.6%.
[f] $\Phi_{\mathbf{5b}}$: 8.3%.
[g] Another prominent emission was detected (Fig. 8).

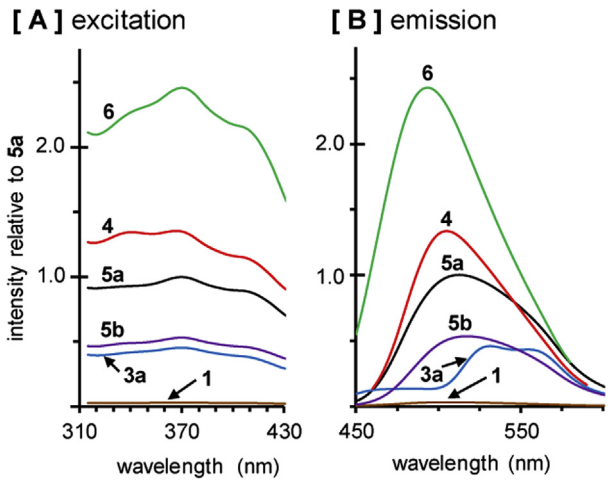

Fig. 7. Spectra of crystalline powders **1**, **3a**, **4**, **5a**, **5b** and **6**. A. Excitation spectra. B. Emission spectra. λ_{ex}: 370 nm for **1**, **5a**, **5b**; 367 nm for **4**, 369 nm for **3a**, 371 nm for **6**.

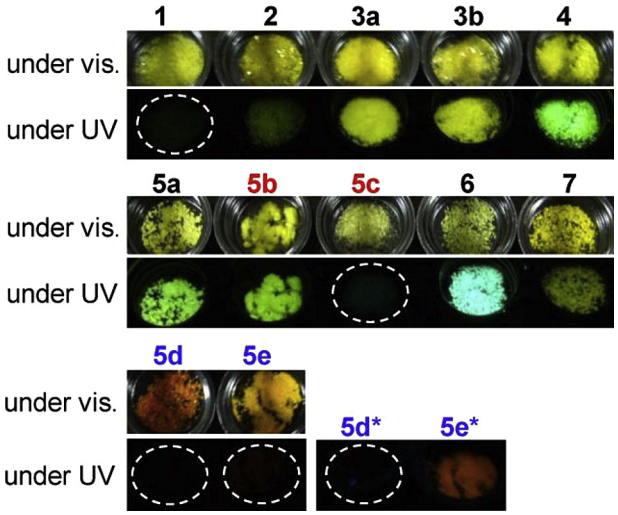

Fig. 6. Real-colour photographs of the fluorescence of crystalline powder DAINs **1**–**7** (black numbers: **1st-DAINs**, red numbers: **2nd-DAINs**, blue numbers: **3rd-DAINs**). The pictures were taken under visible light (top panel) and 365 nm UV lamp (6 W) (bottom panel). The picture with asterisks (*) was obtained with a prolonged shutter speed (× 8).

between 493 and 540 nm. Interestingly, unlike other **1st-DAINs**, imidazoquinoline-type DAINs **3a** and **3b** exhibited another prominent emission in the crystalline powder state at a longer wavelength (λ_{ex}: 477 nm, λ_{em}: 558 nm for **3a**; λ_{ex}: 482 nm, λ_{em}: 559 nm for **3b**) with a good quantum yield ($\Phi_{\mathbf{3a}}$ at λ_{ex}=477 nm: 47.3%). Contour plots of **3a** and **3b**, and their emission spectra corresponding to the longer excitation wavelength are shown in Fig. 8.[18] Because there was no UV–vis absorption at the longer wavelength in the solution state of **3a** and **3b**, (Table 4, runs 3 and 4) the emissions at longer wavelengths were derived from their solid states, probably because of aggregated states, such as a J-aggregate system.[19,20] It also should be noted that with **1st-DAINs**, visible fluorescence emission was observed when the solution was frozen in most cases. Real-colour photographs of the fluorescence from the frozen solutions are shown in Fig. 9A (black numbers correspond to **1st-DAINs**). Visually, emissions ranging from blue to yellow were observed. Interestingly, the emission seemed to depend on the solvent; for example, the emission of **1** was not visible in frozen DMSO, whereas **1** exhibited a blue emission in frozen benzene. Notably, BDI-type compounds were reported to exhibit fluorescence in frozen solutions at low temperatures (in ethanol at −196 °C),[21] whereas DAIN analogues showed fluorescence at higher temperatures ranging from −20 °C (e.g., in DMSO and

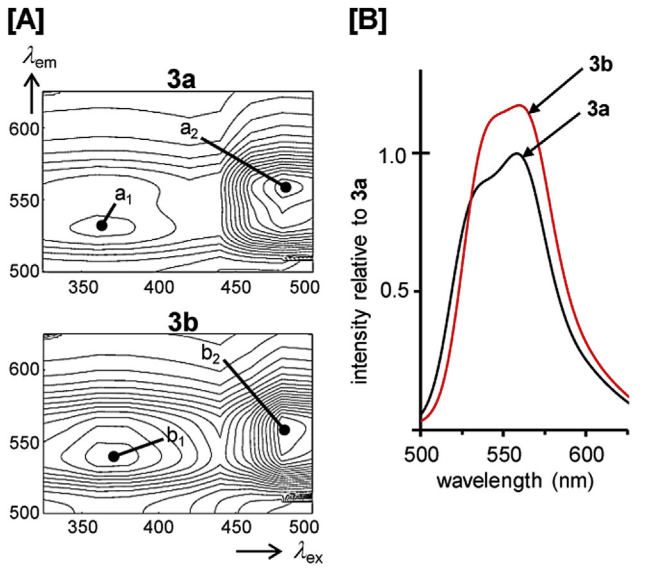

Fig. 8. Dual emission of **3a** and **3b**. A. Excitation–emission contour plots of crystalline powders **3a** and **3b**. (λ_{ex}, λ_{em}): a_1 (369 nm, 531 nm), a_2 (477 nm, 558 nm), b_1 (370 nm, 540 nm), b_2 (482 nm, 559 nm). B. Emission spectra of crystalline powders **3a** and **3b** at the longer excitation wavelength, a_2 and b_2. **3a**: λ_{ex}=477 nm, **3b**: λ_{ex}=482 nm $\Phi_{\mathbf{3a}}$=47.3%, intensity of **3b** relative to **3a**=1.13.

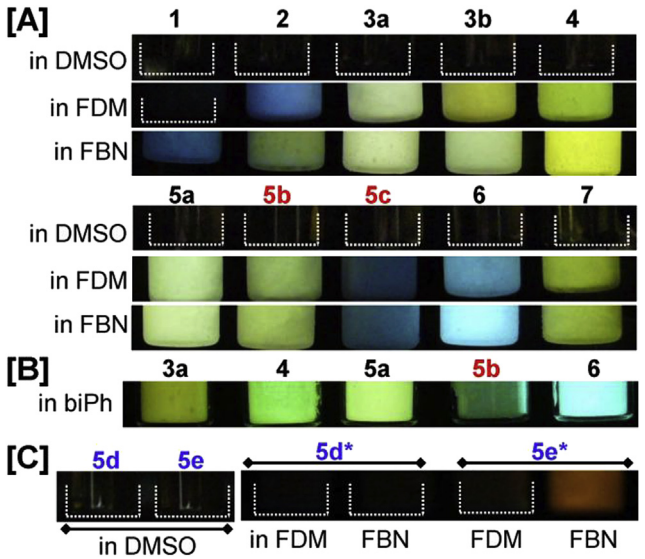

Fig. 9. Real-colour photographs of the fluorescence of DAINs **1**–**7** in solution (black numbers: **1st-DAINs**, red numbers: **2nd-DAINs**, blue numbers: **3rd-DAINs**). A. Pictures of DMSO solutions of **1st-DAINs** and **2nd-DAINs** (1.0×10^{-3} M) under 365 nm UV light (top panel), those of frozen DMSO (FDM) solutions (middle panel) and those of frozen benzene (FBN) solutions (1.0×10^{-3} M) (bottom panel). B. A picture of solidified biphenyl solutions of representative DAINs (1.0×10^{-3} mol/kg) under 365 nm UV light. C. Pictures of DMSO solutions of **3rd-DAINs** (1.0×10^{-3} M) under 365 nm UV light (left panel) and those of FDM and FBN solutions (right panel). The picture with asterisks (*) was obtained with a prolonged shutter speed (× 8). [A–C] The DMSO and benzene solutions were prepared at rt and then frozen at −20 °C. The biphenyl solutions were prepared at 90 °C and then solidified at rt. All photographs were taken under a 365 nm UV lamp (6 W).

benzene) to room temperature (rt) (e.g., in biphenyl, Fig. 9B). Overall, most **1st-DAINs** (e.g., **3**, **4**, **5a** and **6**) exhibited bright fluorescence in the solid state, such as in crystalline powder and in frozen solution, whereas they did not exhibit fluorescence in the solution state. For studies on the second- and third-generation DAINs and as a comparison with the BDI analogues, we selected DAIN **5a** as a model compound of the first-generation DAINs because of its promising solid-state fluorescence (crystalline powder and frozen solution), acceptable quantum yield (16.3%), longer wavelength emission (513 nm) and ease of synthesis.

2.2.1.2. Fluorescence properties of 2nd- and 3rd-generation DAINs. In the solution state (in CH_2Cl_2, benzene and DMSO), the second-generation DAINs **5b** and **5c** (**2nd-DAINs**) and third-generation DAINs **5d** and **5e** (**3rd-DAINs**) were nearly non-fluorescent, similar to the **1st-DAINs**. Moderate emission from the crystalline powder form was observed for one **2nd-DAIN** (**5b**), as shown in Fig. 6 (red numbers for **2nd-DAINs**), Table 5 (run 9) and Fig. 7, although the intensity was lower than that of **5a** (Table 5, run 6). However, the emission of the other **2nd-DAIN** (**5c**) was much weaker (Table 5, run 10). The emission wavelengths of the **2nd-DAINs** were shifted to some extent from that of **5a** (run 6 vs runs 9 and 10). Surprisingly, **3rd-DAINs** were almost non-fluorescent even in the crystalline powder state, although xanthene-containing **5e** emitted a slight orange fluorescence (Fig. 6, blue numbers correspond to **3rd-DAINs**, and Table 5, runs 11 and 12). Similar results were also observed in frozen solutions. In particular, **5b** exhibited visible fluorescence, whereas **5c** and **3rd-DAINs** showed weak or almost no fluorescence (Fig. 9, red numbers for **2nd-DAINs** and blue numbers for **3rd-DAINs**).

*2.2.1.3. Comparison of the fluorescence properties of DAIN **5a** with those of BDIs **8**.* UV–vis absorption and emission spectra in CH_2Cl_2 and emission spectra of the crystalline powder forms of DAIN **5a**, BDIs ***Z*-8** and ***E*-8** are shown in Fig. 10. In solution, the absorption maximum of the longest-wavelength absorption band of DAIN **5a** appeared at a slightly longer wavelength than those of BDIs ***Z*-8** and ***E*-8** (Fig. 10A, λ_{max}: 362, 358 and 359 nm, respectively), even though the molar absorption of **5a** at the absorption maximum was weaker than that of ***Z*-8** (log ε: 4.09 and 4.32, respectively). The fluorescence in solution was quite weak for DAIN **5a** and BDIs **8**, as shown in Fig. 10D; however, emission of BDI ***Z*-8** was somewhat greater ($\Phi_{Z\text{-}8}$: approximately 0.05%) (Fig. 10B). In contrast, the crystalline powder of DAIN **5a** and BDI ***Z*-8** displayed naked-eye visible emission, as shown in Fig. 10E; in this case, DAIN **5a** exhibited a higher quantum yield and a longer emission wavelength than BDI ***Z*-8** ($\Phi_{\mathbf{5a}}$: 16.3%, $\Phi_{Z\text{-}8}$: 1.8%; $\lambda_{em\ \mathbf{5a}}$: 513 nm, $\lambda_{em\ Z\text{-}8}$: 449 nm) (Fig. 10C). Notably, BDI ***E*-8** was almost non-fluorescent even in the crystalline powder state, which may support the 'dark' form of the GFP-chromophore mentioned in the introduction. Although the reason for the non-fluorescence of ***E*-8** is unclear, we suppose that the *E*-phenyl group would be twisted toward the imidazolinone moiety due to steric hindrance, similar to nonfluorescent *E*-BDI type chromoproteins.[22] Overall, it appears that the DAIN structure possessed superior fluorescence properties in the solid state to the corresponding BDI structures in terms of the higher quantum yield and longer emission wavelength. Therefore, the DAIN displayed better 'off' to 'on' fluorescence upon changing from the solution to the solid state.

2.2.2. Discussion

2.2.2.1. Fluorescence properties of the DAIN series. 2.2.2.1.1. In the solution state. To our surprise, all compounds, regardless of generation, were nearly non-fluorescent in the solution state. This result would suggest that the excited energy was consumed by molecular motions, even in the case of DAIN, similar to the case with BDI. Although the photoinduced transformation from the *Z*-to *E*-isomer was excluded in the DAINs, the double bond isomerization at the diarylmethylene moiety probably occurred continuously, similar to a molecular motor. In fact, some compounds with a diarylmethylene group are known to work as light-driven

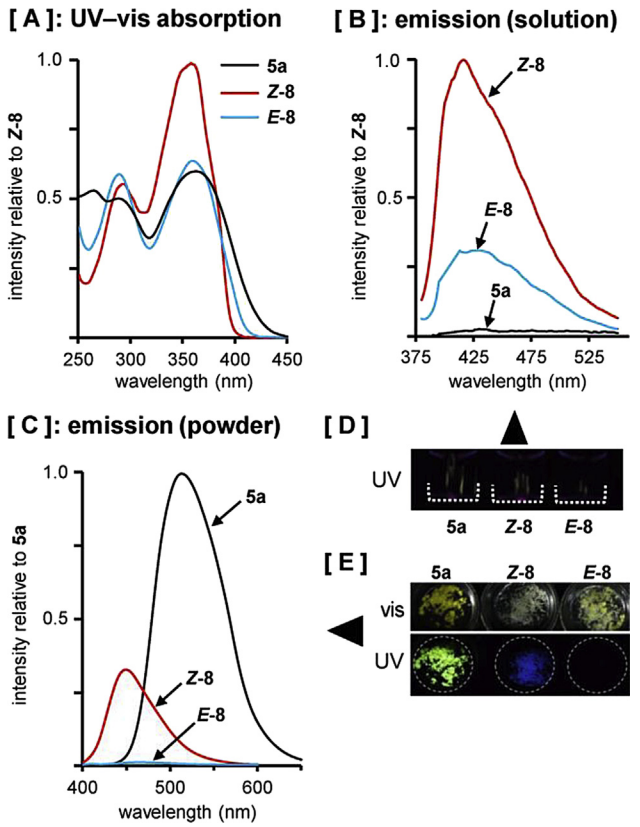

Fig. 10. A. UV–vis absorption spectra for **5a**, ***Z*-8** and ***E*-8** in CH_2Cl_2 solution (1.0×10^{-5} M). λ_{max}: **5a**=362 nm (log ε: 4.09), ***Z*-8**=358 nm (log ε: 4.32), ***E*-8**=359 nm (log ε: 4.13). B. Emission spectra for **5a**, ***Z*-8** and ***E*-8** in CH_2Cl_2 solution (1.0×10^{-5} M). Scattered light (approximately 400–405 nm) was eliminated. The λ_{max} of UV–vis absorption was used as the excitation wavelength for all compounds. λ_{em}: **5a**=432 nm, ***Z*-8**=416 nm, ***E*-8**=429 nm. $\Phi_{Z\text{-}8}$: approximately 0.05%. C. Emission spectra for **5a**, ***Z*-8** and ***E*-8** in the crystalline powder state. λ_{em}: **5a**=513 nm (λ_{ex} 370 nm), ***Z*-8**=449 nm (λ_{ex} 371 nm), ***E*-8**=465 nm (λ_{ex} 370 nm). Φ_{5a}: 16.3%, $\Phi_{Z\text{-}8}$: 1.8%. D. A photograph of the CH_2Cl_2 solution of **5a**, ***Z*-8** and ***E*-8** under a UV lamp (365 nm, 6 W). [E] A photograph of the crystalline powder of **5a**, ***Z*-8** and ***E*-8** under visible light (top panel) and 365 nm UV lamp (6 W) (bottom panel).

molecular motors.[23] Fluorescence quenching caused by twisted intramolecular charge transfer (TICT) at the olefin moiety in the DAIN structure may also be conceivable.[24] In the case of the first- and second-generation DAINs, energy consumption by the single-bond rotations of the aryl–alkene bonds in the diaryl moiety was also possible in addition to the double bond rotation, which would be supposable from the structural similarity between BDI[3] and DAIN. Overall, the emission of all DAIN analogues was nearly non-existent in the solution state, including the third-generation DAINs, which had rigid and flat conformations.

2.2.2.1.2. In the solid state. In contrast, several DAIN analogues exhibited naked-eye visible bright emission in the crystalline powder state (so-called aggregation-induced emission[19,25]) and in frozen solution. The emission from such solid states may have been produced by the restraint of the molecular motions, which would lead to a decrease in the non-radiative energy consumption. With regard to **1st-DAINs**, we initially postulated that a fused benzene ring conjugated to the imidazolinone ring would be important for substantial emission (Table 5, runs 1–5).[11] However, further trials revealed that such a structure was not essential. Compounds **5a** and **7** showed suitable emission without the benzene ring or fused ring structure, respectively (Table 5, runs 6 and 8). Interestingly, modification of the diaryl moiety (i.e., **2nd-** and **3rd-DAINs**) led to reduced emission in the solid state (Table 5, run 6 vs runs 9–12). The substituent effect on the diphenyl moiety seemed to have a negative effect on the emission intensity, regardless of electron donating (–OMe, **5b**) or withdrawing (–Cl, **5c**) ability, whereas the emission wavelength was slightly red-shifted for electron donating **5b** and blue-shifted for electron withdrawing **5c** (run 6 vs runs 9 and 10). To our surprise, the bridging modification at the diaryl moiety (i.e., **3rd-DAINs**) was ineffective even in the solid state, despite the restraint of the carbon–carbon double bond rotation in the solid in addition to the rigid and flat structure (runs 11 and 12). As such, the fluorescence of the DAIN analogues in the solid state probably depended on several factors; for example, not only the conformation and electron density of the molecule, but also the degree of vibrations and its surrounding conditions in the solid state can be contributing factors. However, the restraint of molecular motions seemed to be the most crucial factor. Details regarding the crystalline conditions are discussed in Sections 2.2.2.2 and 2.2.2.3.

Overall, the observed fluorescence properties of the DAIN series differed significantly from our initial expectations; however, it is noteworthy that DAINs, particularly non-bridged DAINs, have a useful function in that their fluorescence is turned 'on' when their molecular motions are restrained. Although BDI analogues exhibit a similar off/on property, DAINs possessed a superior off/on effect in that the DAIN showed lower fluorescence (i.e., 'off') in solution (Fig. 10B) and a higher fluorescence (i.e., 'on') in the solid state (Fig. 10C). Accordingly, DAINs could be utilised in fluorescence off/on switching systems by controlling their molecular motions.

2.2.2.2. Conformational analysis of DAINs with X-ray crystal structures. The X-ray crystal structures of representative DAINs **1**, **3a**, **5d** and **6** are shown in Fig. 11.[26] It has been reported that the phenyl and imidazolinone (IMN) rings in BDI, including in GFP,[2] are almost coplanar in the crystalline state (Fig. 12).[27] In contrast, the diphenyl moiety in DAIN, except for fluorine-containing **5d**, exhibited a twisted conformation, as shown in Table 6. Although the torsion between *Z*-Ph and IMN was somewhat less (approximately 30–40°) than that between *E*-Ph and IMN (approximately 60–70°), it was not as flat as that of BDI. Nonetheless, some conjugation seemed to exist between the *Z*-Ph and IMN moieties in DAIN, when considering the fluorescence properties of DAIN and BDI, as mentioned above. In contrast, **5d** exhibited a planar conformation, as expected. Therefore, factors other than its conformation must be considered to explain the very weak fluorescence of the crystalline powder form of **5d**.

2.2.2.3. Molecular packing analysis of X-ray crystal structures of DAINs. To obtain a better understanding of the fluorescence of the crystalline powder form of DAINs, molecular packing analysis of the X-ray crystal structures was performed with fluorescent DAINs **3a** and **6**, and nearly non-fluorescent DAINs **1** and **5d**. A remarkable difference between the fluorescent and non-fluorescent DAINs was found in their space groups, as shown in Fig. 13. Fluorescent compounds **3a** and **6** belonged to the $P2_1/c$ group (top two panels), while non-fluorescent **1** and **5d** belonged to other groups, such as *P*-1 and *C*2/*c* (bottom two panels). Regarding solid-state fluorescence, it is known that intermolecular π–π interactions typically lead to fluorescence quenching (non-radiative process) because of electron and/or energy transfers.[19,28] The molecular packing of non-fluorescent DAINs **1** and **5d** appeared to lead to such quenching. In both cases, neighbouring molecules were packed in an anti-parallel fashion and the π-bonds overlapped each other within 3.6–5.0 Å, which would be close enough for such transfers via the Dexter mechanism, as shown in Fig. 14. These compounds might be forming excimers with an intermolecular distance of approximately 3.6–3.7 Å, resulting in the quenched emission.[29] In contrast, fluorescent DAINs **3a** and **6** were packed in a stepwise form with a head-to-tail configuration, as shown in Fig. 15.

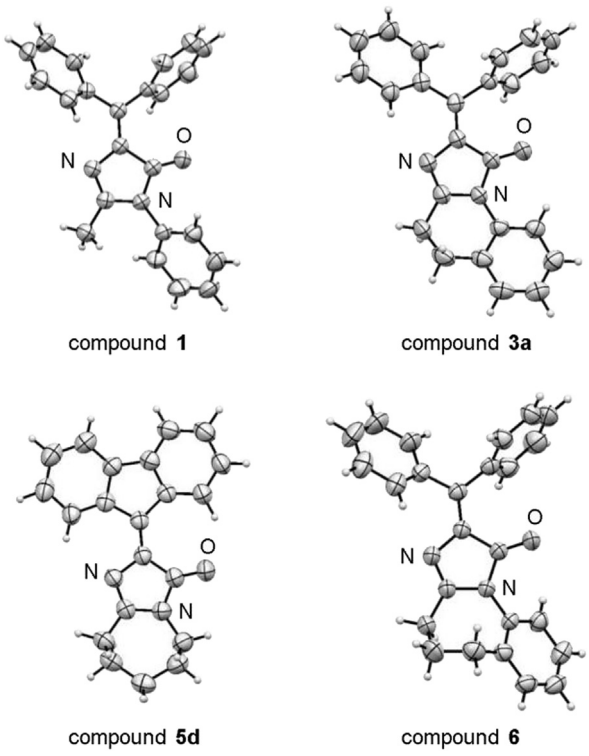

Fig. 11. X-ray-based ORTEP drawings of **1**, **3a**, **5d** and **6**. Ellipsoids are set at 50% probability.[26]

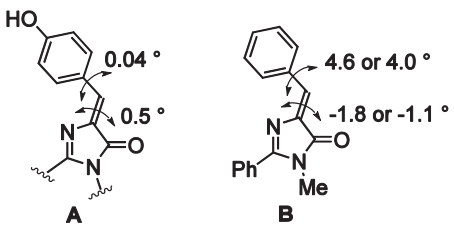

Fig. 12. Torsion angles in BDI structures. A: HO-BDI in GFP structure (PDBID: 1GFL); B: Reported by Ramanathan et al.[27]

Although the molecules overlapped within 4.0–4.5 Å in the lattices, effective π–π interactions probably did not arise because of the non-overlapping or non-parallel arrangement of the aromatic rings. However, the difference in the spacing between the layers may explain the different emission colours (i.e., **3a**: 3.95 Å, yellow fluorescence; **6**: 4.51 Å, cyan fluorescence).[30]

Table 6
Torsion angle (°) between the C–Ph bond (φ) and the C=C bond (τ) measured from the ORTEP drawings

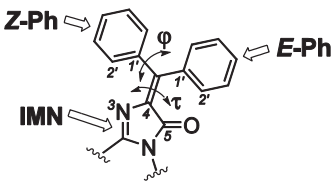

DAIN[a]	φ (Z-Ph)[b]	φ (E-Ph)[b]	τ(Z)[c]	τ(E)[d]
1	42.4	59.1	5.7	9.6
3a	31.4	71.4	3.4	1.5
5d	3.5	−6.1	−3.2	−2.5
6	40.8	63.9	7.7	8.2

[a] Angles were measured for one of the enantiomeric structures in the unit cell.
[b] Torsion of C(4)=C–C(1′)–C(2′).
[c] Torsion of N(3)–C(4)=C–C(1′).
[d] Torsion of C(5)–C(4)=C–C(1′).

3. Conclusions

Synthesis—The newly designed GFP chromophore analogues, DAINs, were successfully synthesized using a novel condensation reaction between (thio)imidate **9** and *N*-(diarylmethylene)glycinate **10**. This reaction proceeded smoothly under weakly acidic conditions in refluxing toluene or, in some cases, at room temperature. Although both thioimidates and imidates were viable components in this reaction, imidates appeared to afford a better yield in a shorter reaction time. This reaction was affected by properties of the diarylmethylene moiety; the stability of the benzylic carbocation at the diarylmethylene moiety seemed to influence the reactivity. The reaction mechanism included an unprecedented migration step of the diarylmethylene group from the nitrogen to α-carbon probably via an aziridine intermediate.

Fluorescence properties—The DAINs possessed interesting fluorescence properties. They were nearly non-fluorescent in the solution state regardless of their bridged or non-bridged structure at the diarylmethylene moiety. This result would suggest that the excited energy was consumed by molecular motions such as the continuous photo-induced carbon–carbon double bond rotation at the diarylmethylene moiety, similar to a light-driven molecular motor, and the single-bond rotations of the aryl–alkene moieties. In contrast, naked-eye visible fluorescence emission was detected in the crystalline powder state and the frozen solution state of many DAINs. This was probably because of a decrease in the energy consumption owing to the restrained molecular motions. Thus, the restraint of molecular motions is crucial to the emission of DAIN analogues. In addition, regarding the solid-state fluorescence, the crystal packing of the molecules was also important. The non-fluorescent analogues **1** and **5d** seemed to exhibit intermolecular π–π interactions, which would cause fluorescence quenching by electron and/or energy transfers, whereas the fluorescent analogues **3a** and **6** exhibited a stepwise arrangement where such π–π interactions did not seem to exist. Comparison of the solid-state fluorescence properties of DAIN **5a** with those of the corresponding BDIs **8** showed that the DAIN structure possessed superior properties in terms of the higher quantum yield and the longer emission wavelength. Although some properties of the DAIN analogues differed from our initial expectations, they would be of great use in a fluorescence off/on switching system where the restraint of the molecular motion is applicable to the switch mechanism. Studies on such applications are now in progress in our laboratory.

4. Experimental section

4.1. General information

^{1}H and ^{13}C NMR spectra were recorded on a JEOL JNM-AL400 spectrometer (400 and 100 MHz, respectively); the chemical shifts are reported in parts per million (ppm) relative to tetramethylsilane or solvent signals ($CDCl_3$: 7.26 ppm for ^{1}H- and 77.0 ppm for ^{13}C NMR; DMSO-d_6: 2.50 ppm for ^{1}H- and 39.5 ppm for ^{13}C NMR; C_6D_6: 7.16 ppm for ^{1}H NMR; acetone-d_6: 2.05 ppm for ^{1}H NMR; CD_3CN: 1.94 ppm for ^{1}H NMR; CD_2Cl_2: 53.8 ppm for ^{13}C NMR). Mass spectra were recorded using a JEOL JMS-BU25 mass spectrometer in positive FAB mode or using a JEOL JMS-T100GCV mass spectrometer in positive FD mode. UV–vis spectra were obtained on a SHIMADZU MultiSpec-1500 spectrophotometer at concentrations of 1.0×10^{-5} M in CH_2Cl_2. IR spectra were obtained on a JASCO FT/IR-6300 spectrometer by diffuse reflection in KBr. Melting points (Mp) were measured using a Yanaco melting-point apparatus and are uncorrected. Microanalyses were performed by

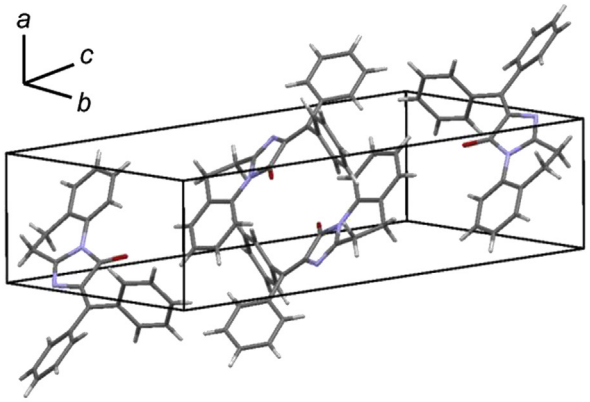

compound **3a**:
space group: $P2_1/c$
cell lengths: *a* 5.99198(11), *b* 12.0940(2), *c* 24.5614(5)
cell angles: α 90.0000, β 90.8124(9), γ 90.0000
Z: 4

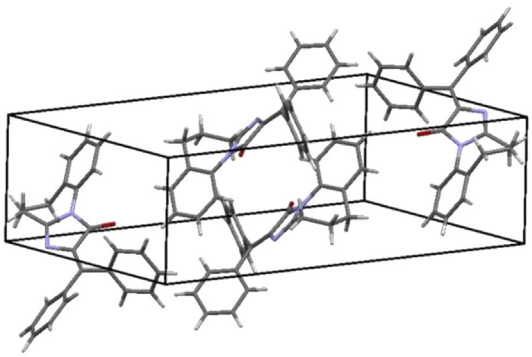

compound **6**:
space group: $P2_1/c$
cell lengths: *a* 6.52704(12), *b* 12.4742(2), *c* 23.7463(4)
cell angles: α 90.0000, β 91.9997(7), γ 90.0000
Z: 4

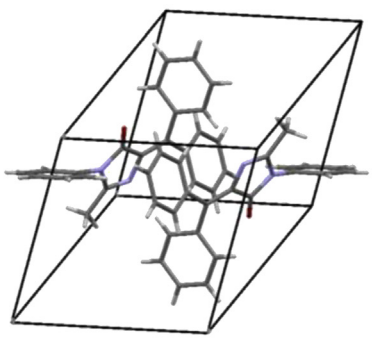

compound **1**:
space group: *P*-1
cell lengths: *a* 9.62064(17), *b* 10.12554(18), *c* 10.4363(8)
cell angles: α 89.495(7), β 75.662(6), γ 67.110(5)
Z: 2

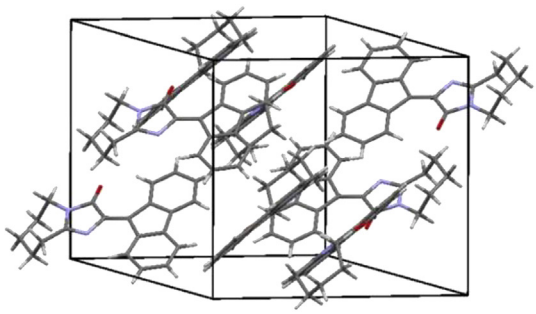

compound **5d**:
space group: *C*2/*c*.
cell lengths: *a* 13.0456(3) *b* 15.6030(3) *c* 15.8625(3)
cell angles: α 90.0000 β 93.6563(10) γ 90.0000
Z: 8

Fig. 13. X-ray crystal structures and space groups of fluorescent DAINs **3a** and **6**, and nearly non-fluorescent DAINs **1** and **5d**. Lengths in Å, angles in °.

A Rabbit Science Japan Co., Ltd. (Sagamihara, Japan). Fluorescence spectra were recorded using a JASCO FP-6200 spectrofluorometer equipped with an FPA-450 solid sample attachment to measure the fluorescence of crystalline powder samples. Quantum yield measurements of solid samples were carried out by JASCO Corporation (Tokyo, Japan) or performed on a JASCO FP-8300 spectrometer. X-ray diffraction measurements were performed on a Rigaku RAXIS-RAPID diffractometer using CuKα radiation. Analytical thin-layer chromatography was carried out on Merck silica gel 60 F_{254}. Column chromatography was performed using a disposable silica gel column RediSep (Teledyne Isco, Inc.) or Fuji Silysia PSQ 100B or Fuji Silysia CHROMATOREX (NH-silica gel).

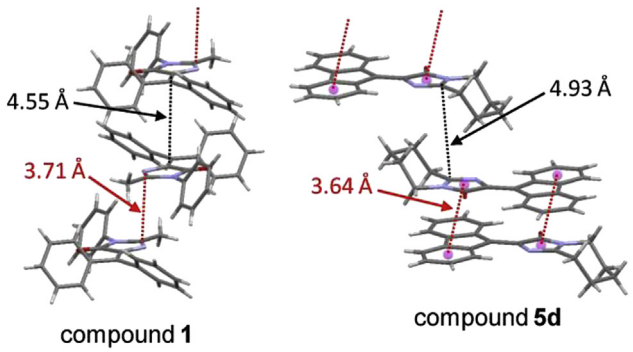

Fig. 14. Intermolecular π–π interactions in nearly non-fluorescent DAINs **1** and **5d**. Dotted lines represent the distances of the π–π interactions.

4.2. General procedure for DAIN synthesis

A mixture of imidate or thioimidate **9** (0.10–1.0 mmol, 1.0 equiv), *N*-(diarylmethylene)glycinate **10** (3.0–5.0 equiv), and acetic acid (2.0–4.0 equiv) in toluene (ca. 0.2 M concentration of the imidate) was stirred under gentle reflux (or at room temperature in some cases) for several hours to days, as shown in Tables 2 and 3. After being cooled to room temperature, the mixture was diluted with ethyl acetate and was washed with a saturated solution of $NaHCO_3$, water, and 10% aqueous HCl. In the case of polar products (e.g., **2**, **4**, **5a**, **5b**, **7**), the acidic aqueous layer was re-extracted with ethyl acetate after neutralization with a saturated solution of $NaHCO_3$. The (combined) organic layers were washed with a saturated solution of $NaHCO_3$ and brine, dried over Na_2SO_4, and concentrated under reduced pressure. The residue was purified by silica gel column chromatography to give DAIN as a coloured solid. The product was recrystallised from dichloromethane/hexane prior to evaluation of its properties.

Please cite this article in press as: Ikejiri, M.; et al., Tetrahedron (2015), http://dx.doi.org/10.1016/j.tet.2015.05.073

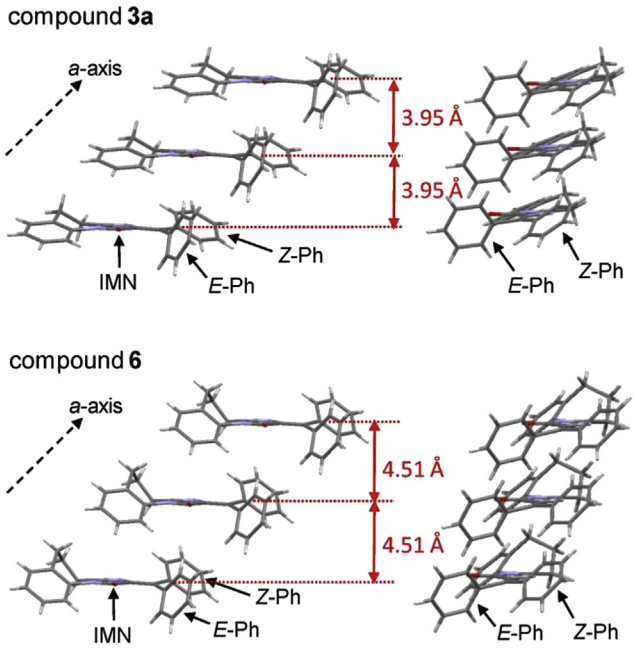

Fig. 15. Head-to-tail configuration of fluorescent DAINs **3a** and **6**. Distances between layers are shown with red arrows.

*4.2.1. 4-(Diphenylmethylene)-2-methyl-1-phenyl-1H-imidazol-5(4H)-one (**1**).* Eluent for silica gel chromatography: ethyl acetate/hexane=1:4 to 1:3. Yellow plates. Mp: 209–210 °C. ^{1}H NMR ($CDCl_3$) δ=7.63–7.61 (m, 2H), 7.46–7.33 (m, 11H), 7.23–7.20 (m, 2H), 2.25 (s, 3H) ppm ^{13}C NMR (CD_2Cl_2) δ=168.1, 160.3, 146.2, 140.1, 138.3, 136.4, 134.2, 132.5, 130.9, 129.7, 129.5, 129.1, 128.8, 128.2, 128.0, 127.8, 16.5 ppm. IR (KBr) ν_{max}: 1620, 1715 cm^{-1}. UV (CH_2Cl_2) λ_{max} nm (log ε): 241 (4.31), 299 (4.15), 357 (4.21). MS (FAB) *m/z* 339 (M+H$^+$). Anal. Calcd for C 81.63, H 5.36, N 8.28; found C 81.45, H 5.28, N 8.27.

*4.2.2. 2-(Diphenylmethylene)-5,6,7,8-tetrahydroimidazo[1,2-a]pyridin-3(2H)-one (**2**).* Eluent for silica gel chromatography: ethyl acetate/hexane=1:4 to 1:2. Yellow needles. Mp: 226–227 °C. ^{1}H NMR ($CDCl_3$) δ=7.56–7.54 (m, 2H), 7.41–7.29 (m, 8H), 3.49 (t, *J*=6 Hz, 2H), 2.80 (t, *J*=6 Hz, 2H), 1.91–1.83 (m, 4H) ppm ^{13}C NMR (CD_2Cl_2) δ=169.1, 161.5, 144.5, 140.2, 138.6, 136.9, 132.4, 130.9, 129.2, 128.9, 128.1, 127.9, 40.2, 26.8, 22.3, 20.4 ppm. IR (KBr) ν_{max}: 1619, 1703 cm^{-1}. UV (CH_2Cl_2) λ_{max} nm (log ε): 264 (3.96), 288 (3.90), 365 (4.00). MS (FAB) *m/z* 303 (M+H$^+$). Anal. Calcd for C 79.44, H 6.00, N 9.26; found C 79.45, H 6.17, N 9.34.

*4.2.3. 2-(Diphenylmethylene)-4,5-dihydroimidazo[1,2-a]quinolin-1(2H)-one (**3a**).* Eluent for silica gel chromatography: ethyl acetate/hexane=1:4 to 1:3. Yellow needles. Mp: 210.5–211.5 °C. ^{1}H NMR ($CDCl_3$) δ=8.27 (d, *J*=8 Hz, 1H), 7.58–7.55 (m, 2H), 7.47–7.34 (m, 8H), 7.24–7.21 (m, 2H), 7.11 (td, *J*=7, 1 Hz, 1H), 3.01 (s, 4H). ^{1}H NMR (C_6D_6) δ=8.55 (dd, *J*=8, 1 Hz, 1H), 7.85–7.82 (m, 2H), 7.42–7.39 (m, 2H), 7.28–7.06 (m, 6H), 7.01 (td, *J*=8, 2 Hz, 1H), 6.81 (td, *J*=7, 1 Hz, 1H), 6.71 (dd, *J*=8, 1 Hz, 1H), 2.31 (dd, *J*=8, 6 Hz, 2H), 2.15 (dd, *J*=8, 6 Hz, 2H) ppm ^{13}C NMR (CD_2Cl_2) δ=166.0, 160.3, 146.8, 140.0, 138.4, 136.6, 134.1, 132.4, 130.8, 129.6, 129.2, 128.7, 128.3, 128.0, 127.9, 126.8, 125.4, 117.7, 26.3, 25.8 ppm. IR (KBr) ν_{max}: 1634, 1710 cm^{-1}. UV (CH_2Cl_2) λ_{max} nm (log ε): 249 (4.41), 313 (4.32), 370 (3.95). MS (FAB) *m/z* 351 (M+H$^+$). Anal. Calcd for C 82.26, H 5.18, N 7.99; found C 82.26, H 5.26, N 7.98.

*4.2.4. 2-(Diphenylmethylene)-7-methoxy-4,5-dihydroimidazo[1,2-a]quinolin-1(2H)-one (**3b**).* Eluent for silica gel chromatography: ethyl acetate/CH_2Cl_2=1:50. Yellow needles. Mp: 202–202.5 °C. ^{1}H NMR (C_6D_6) δ=8.51 (d, *J*=9 Hz, 1H), 7.86 (d, *J*=8 Hz, 2H), 7.44 (d, *J*=8 Hz, 2H), 7.28–7.21 (m, 4H), 7.11–7.06 (m, 2H), 6.56 (dd, *J*=9, 3 Hz, 1H), 6.51 (d, *J*=3 Hz, 1H), 3.24 (s, 3H), 2.33 (t, *J*=7 Hz, 2H), 2.14 (t, *J*=7 Hz, 2H) ppm ^{13}C NMR (CD_2Cl_2) δ=165.9, 160.4, 157.1, 146.6, 140.0, 138.4, 136.8, 132.4, 130.9, 129.5, 129.1, 128.3, 128.2, 128.0, 127.6, 118.7, 114.4, 112.5, 55.8, 26.5, 25.8 ppm. IR (KBr) ν_{max}: 1637, 1708 cm^{-1}. UV (CH_2Cl_2) λ_{max} nm (log ε): 254 (4.45), 320 (4.36), 390 (3.72). MS (FAB) *m/z* 381 (M+H$^+$). Anal. Calcd for C 78.93, H 5.30, N 7.36; found C 78.64, H 4.94, N 7.61.

*4.2.5. 2-(Diphenylmethylene)-5,6-dihydroimidazo[2,1-a]isoquinolin-3(2H)-one (**4**).* Eluent for silica gel chromatography: ethyl acetate/hexane=1:10 to 1:4. Yellow needles. Mp: 163.5–164.5 °C. ^{1}H NMR ($CDCl_3$) δ=8.23 (d, *J*=8 Hz, 1H), 7.73–7.70 (m, 2H), 7.51–7.34 (m, 11H), 7.30 (d, *J*=8 Hz, 1H), 3.81 (t, *J*=7 Hz, 2H), 3.10 (t, *J*=7 Hz, 2H) ppm ^{13}C NMR (CD_2Cl_2) δ=168.0, 156.2, 145.9, 140.2, 138.7, 138.5, 137.9, 132.9, 132.6, 131.1, 129.5, 129.1, 128.8, 128.2, 128.0, 127.8, 126.5, 125.4, 37.2, 28.2 ppm. IR (KBr) ν_{max}: 1620, 1706 cm^{-1}. UV (CH_2Cl_2) λ_{max} nm (log ε): 268 (4.45), 310 (4.13), 397 (4.34). MS (FAB) *m/z* 351 (M+H$^+$). Anal. Calcd for C 82.26, H 5.18, N 7.99; found C 82.25, H 5.22, N 7.96.

*4.2.6. 2-(Diphenylmethylene)-6,7,8,9-tetrahydro-2H-imidazo[1,2-a]azepin-3(5H)-one (**5a**).* Eluent for silica gel chromatography: ethyl acetate/hexane=1:3 to 1:2. Yellow needles. Mp: 194–195 °C. ^{1}H NMR ($CDCl_3$) δ=7.58–7.55 (m, 2H), 7.41–7.26 (m, 8H), 3.63–3.61 (br m, 2H), 2.79–2.73 (br m, 2H), 1.84–1.74 (br m, 4H), 1.69–1.60 (br m, 2H) ppm ^{13}C NMR (CD_2Cl_2) δ=168.2, 166.5, 145.2, 140.2, 138.7, 137.5, 132.4, 130.8, 129.2, 128.9, 128.1, 127.9, 40.8, 31.8, 31.1, 29.4, 26.1 ppm. IR (KBr) ν_{max}: 1623, 1700 cm^{-1}. UV (CH_2Cl_2) λ_{max} nm (log ε): 265 (4.02), 287 (4.00), 362 (4.09). MS (FAB) *m/z* 317 (M+H$^+$). Anal. Calcd for C 79.72, H 6.37, N 8.85; found C 79.72, H 6.44, N 8.64.

*4.2.7. 2-(Diphenylmethylene)-2,4,5,6-tetrahydro-1H-benzo[f]imidazo[1,2-a]azepin-1-one (**6**).* Eluent for silica gel chromatography: ethyl acetate/hexane=1:9 to 1:4. Yellow needles. Mp: 213.5–214 °C. ^{1}H NMR ($CDCl_3$) δ=7.63–7.60 (m, 2H), 7.45 (d, *J*=8 Hz, 1H), 7.42–7.34 (m, 8H), 7.31–7.20 (m, 3H), 2.74 (t, *J*=7 Hz, 2H), 2.69 (t, *J*=7 Hz, 2H), 2.24–2.17 (m, 2H) ppm ^{13}C NMR (CD_2Cl_2) δ=166.7, 162.9, 146.7, 140.1, 138.4, 136.7, 135.0, 134.0, 132.5, 130.9, 130.1, 129.5, 129.2, 128.2, 128.0, 127.8, 127.6, 124.8, 30.5, 27.3, 27.2 ppm. IR (KBr) ν_{max}: 1625, 1712 cm^{-1}. UV (CH_2Cl_2) λ_{max} nm (log ε): 244 (4.36), 306 (4.24), 367 (4.10). MS (FAB) *m/z* 365 (M+H$^+$). Anal. Calcd for C 82.39, H 5.53, N 7.69; found C 82.43, H 5.54, N 7.64.

*4.2.8. 4-(Diphenylmethylene)-1-methyl-2-phenyl-1H-imidazol-5(4H)-one (**7**).* Eluent for silica gel chromatography: ethyl acetate/hexane=1:9 to 1:4. Yellow needles. Mp: 208.5–209.5 °C. ^{1}H NMR ($CDCl_3$) δ=7.83–7.81 (m, 2H), 7.70–7.67 (m, 2H), 7.55–7.51 (m, 3H), 7.46–7.43 (m, 3H), 7.38–7.35 (m, 5H), 3.28 (s, 3H) ppm ^{13}C NMR (CD_2Cl_2) δ=169.7, 161.5, 147.0, 140.0, 138.6, 137.2, 132.9, 131.5, 131.0, 130.0, 129.6, 129.2, 129.1, 128.9, 128.2, 128.0, 29.1 ppm. IR (KBr) ν_{max}: 1616, 1707 cm^{-1}. UV (CH_2Cl_2) λ_{max} nm (log ε): 258 (4.34), 296 (4.04), 390 (4.17). MS (FAB) *m/z* 339 (M+H$^+$). Anal. Calcd for C 81.63, H 5.36, N 8.28; found C 81.85, H 5.43, N 8.13.

*4.2.9. 2-(Bis(4-methoxyphenyl)methylene)-6,7,8,9-tetrahydro-2H-imidazo[1,2-a]azepin-3(5H)-one (**5b**).* Eluent for silica gel chromatography: ethyl acetate/hexane=2:3 to 1:1. Yellow needles. Mp: 209.5–210.5 °C. ^{1}H NMR ($CDCl_3$) δ=7.53 (d, *J*=9 Hz, 2H), 7.26 (d, *J*=9 Hz, 2H), 6.92 (d, *J*=9 Hz, 2H), 6.87 (d, *J*=9 Hz, 2H), 3.85 (s, 3H), 3.83 (s, 3H), 3.68–3.62 (br m, 2H), 2.80–2.75 (br m, 2H), 1.85–1.74 (br m, 4H), 1.71–1.62 (br m, 2H) ppm ^{13}C NMR (CD_2Cl_2) δ=168.2, 164.8, 160.8, 160.7, 145.6, 135.9, 134.5, 132.9, 130.9, 113.4, 113.3, 55.7, 55.6, 40.7, 31.8, 31.1, 29.5, 26.2 ppm. IR (KBr) ν_{max}: 1601, 1696 cm^{-1}.

Please cite this article in press as: Ikejiri, M.; et al., Tetrahedron (2015), http://dx.doi.org/10.1016/j.tet.2015.05.073

UV (CH_2Cl_2) λ_{max} nm (log ε): 318 (4.18), 384 (4.27). MS (FAB) *m/z* 377 ($M+H^+$). Anal. Calcd for C 73.38, H 6.43, N 7.44; found C 73.20, H 6.46, N 7.41.

*4.2.10. 2-(Bis(4-chlorophenyl)methylene)-6,7,8,9-tetrahydro-2H-imidazo[1,2-a]azepin-3(5H)-one (**5c**).* During the work-up, the mixture was not washed with aqueous HCl. Eluent for silica gel chromatography: ethyl acetate/hexane=1:4 to 1:3. Pale yellow needles. Mp: 187.5–188.5 °C. ^{1}H NMR ($CDCl_3$) δ=7.51 (d, *J*=9 Hz, 2H), 7.38 (d, *J*=9 Hz, 2H), 7.32 (d, *J*=9 Hz, 2H), 7.23 (d, *J*=9 Hz, 2H), 3.67–3.60 (br m, 2H), 2.80–2.75 (br m, 2H), 1.85–1.76 (br m, 4H), 1.69–1.66 (br m, 2H) ppm ^{13}C NMR (CD_2Cl_2) δ=168.0, 167.4, 141.9, 138.1, 137.9, 136.6, 135.4, 135.0, 133.9, 132.4, 128.5, 128.2, 40.8, 31.8, 31.0, 29.3, 26.0 ppm. IR (KBr) ν_{max}: 1619, 1705 cm^{-1}. UV (CH_2Cl_2) λ_{max} nm (log ε): 274 (4.25), 370 (4.21). MS (FAB) *m/z* 385 ($M+H^+$). Anal. Calcd for C 65.46, H 4.71, N 7.27; found C 65.18, H 4.55, N 7.23.

*4.2.11. 2-(9H-Fluoren-9-ylidene)-6,7,8,9-tetrahydro-2H-imidazo[1,2-a]azepin-3(5H)-one (**5d**).* Eluent for silica gel chromatography: ethyl acetate/hexane=1:20 to 1:8. Ruby red prisms. Mp: 192.5–193.5 °C. ^{1}H NMR ($CDCl_3$) δ=9.45 (d, *J*=8 Hz, 1H), 9.01 (d, *J*=8 Hz, 1H), 7.63–7.59 (m, 2H), 7.40–7.27 (m, 4H), 3.85–3.77 (br m, 2H), 2.92–2.86 (br m, 2H), 1.93–1.83 (br m, 4H), 1.80–1.71 (br m, 2H). ^{1}H NMR (acetone-d_6) δ=9.52 (dd, *J*=8, 1 Hz, 1H), 9.09 (dd, *J*=8, 1 Hz, 1H), 7.78 (d, *J*=8 Hz, 1H), 7.75 (d, *J*=8 Hz, 1H), 7.43 (td, *J*=8, 1 Hz, 1H), 7.39 (td, *J*=8, 1 Hz, 1H), 7.33 (td, *J*=8, 1 Hz, 1H), 7.30 (td, *J*=8, 1 Hz, 1H), 3.84 (br t, *J*=5 Hz, 2H), 2.96–2.92 (m, 2H), 1.94–1.85 (m, 4H), 1.80–1.74 (m, 2H) ppm ^{13}C NMR (CD_2Cl_2) δ=169.0, 167.6, 142.3, 142.2, 139.8, 139.2, 138.4, 136.6, 131.3, 130.9, 130.4, 129.3, 128.3, 127.9, 119.8, 119.7, 41.1, 32.2, 31.1, 29.4, 26.1 ppm. IR (KBr) ν_{max}: 1601, 1626, 1696 cm^{-1}. UV (CH_2Cl_2) λ_{max} nm (log ε): 242 (4.56), 267 (4.59), 275 (4.64), 333 (4.01)., 406 (4.39). MS (FAB) *m/z* 315 ($M+H^+$). Anal. Calcd for C 80.23, H 5.77, N 8.91; found C 80.10, H 5.70, N 8.85.

*4.2.12. 2-(9H-Xanthen-9-ylidene)-6,7,8,9-tetrahydro-2H-imidazo[1,2-a]azepin-3(5H)-one (**5e**).* Eluent for silica gel chromatography: ethyl acetate/hexane=1:4. Orange powder. Mp: 193.5–194 °C. ^{1}H NMR ($CDCl_3$) δ=8.98 (dd, *J*=8, 1 Hz, 1H), 8.43 (dd, *J*=8, 1 Hz, 1H), 7.48–7.39 (m, 2H), 7.29–7.20 (m, 4H), 3.71–3.68 (br m, 2H), 2.81–2.78 (br m, 2H), 1.85–1.77 (br m, 4H), 1.71–1.64 (br m, 2H) ppm ^{13}C NMR (CD_2Cl_2) δ=167.8, 164.5, 153.7, 153.4, 133.5, 131.9, 131.8, 131.4, 131.2, 130.7, 123.3, 123.2, 122.1, 119.7, 116.5, 116.4, 41.0, 31.9, 31.1, 29.4, 26.2 ppm. IR (KBr) ν_{max}: 1605, 1688 cm^{-1}. UV (CH_2Cl_2) λ_{max} nm (log ε): 295 (4.15), 412 (4.29). MS (FAB) *m/z* 331 ($M+H^+$). Anal. Calcd for C 76.34, H 5.49, N 8.48; found C 76.04, H 5.45, N 8.47.

4.3. Synthesis of BDIs 8

*4.3.1. 1-(2-Azidoacetyl)azepan-2-one (**14**).* To a stirred solution of **12** (2.00 g, 17.7 mmol) in CH_2Cl_2 (44 mL), triethylamine (2.71 mL, 19.5 mmol) and 2-chloroacetyl chloride (1.55 mL, 19.5 mmol) were added at room temperature, and stirred at room temperature for 2 h. After dilution of the mixture with ethyl acetate, the organic layer was washed with water, and brine, then dried over Na_2SO_4, and concentrated under reduced pressure. The residue was subjected to the next reaction without purification. To a stirred solution of crude **13** (ca. 2.2 g) in DMSO (44 mL), NaN_3 (2.30 g, 35.4 mmol) was added at room temperature, and stirred overnight at room temperature. After dilution of the mixture with ether, the organic layer was washed with water and brine, dried over $MgSO_4$, and concentrated under reduced pressure to afford **14** (1.13 g, 33% from **12**) as an almost pure compound. ^{1}H NMR ($CDCl_3$) δ=4.43 (s, 2H), 3.98–3.95 (m, 2H), 2.74–2.71 (m, 2H), 1.82–1.70 (m, 6H) ppm ^{13}C NMR ($CDCl_3$) δ=177.8, 171.1, 55.9, 43.6, 39.2, 29.0, 28.3, 23.5 ppm. IR (KBr) ν_{max}: 1699, 2107 cm^{-1}. HRMS (FAB) Calcd for $C_8H_{13}N_4O_2$ ($M+H^+$): 197.1038. Found: 197.1030.

*4.3.2. 6,7,8,9-Tetrahydro-2H-imidazo[1,2-a]azepin-3(5H)-one (**15**).*[16]

*4.3.2.1. Synthesis from **14**.* To a stirred solution of **14** (560 mg, 2.86 mmol) in toluene (14 mL), Ph_3P (825 mg, 3.15 mmol) was added at room temperature, and stirred at room temperature for 2.5 h. After evaporation of the solvent, the residue was purified by silica gel column chromatography (ethyl acetate, then $CHCl_3$/MeOH=10/1) to give **15** (390 mg, 90%) as a yellow oil.

*4.3.2.2. Synthesis from **9**.* To a stirred solution of **9** (500 mg, 3.94 mmol) in MeOH (30 mL), triethylamine (1.10 mL, 7.88 mmol) and glycine methyl ester hydrochloride (993 mg, 7.91 mmol) were added at room temperature; the mixture was stirred under reflux for 1.5 h. Subsequent to evaporation of the solvent, the residue was dissolved in ether, and the precipitate was removed by filtration. After concentration of the filtrate, the residue was purified by silica gel column chromatography ($CHCl_3$/MeOH=30/1) to give **15** (576 mg, 96%) as a yellow oil. ^{1}H NMR ($CDCl_3$) δ=4.10 (t, *J*=1 Hz, 2H), 3.66–3.57 (m, 2H), 2.71–2.62 (m, 2H), 1.84–1.58 (m, 6H) ppm ^{13}C NMR ($CDCl_3$) δ=180.5, 168.4, 58.7, 40.4, 31.7, 30.5, 29.1, 25.4 ppm. IR (KBr) ν_{max}: 1634, 1724 cm^{-1}. HRMS (FAB) Calcd for $C_8H_{13}N_2O$ ($M+H^+$): 153.1028. Found: 153.1040.

*4.3.3. (Z)-2-Benzylidene-6,7,8,9-tetrahydro-2H-imidazo[1,2-a]azepin-3(5H)-one (**Z-8**).* To a stirred solution of **15** (1.00 g, 6.58 mmol) in MeOH (50 mL), benzaldehyde (734 μL, 7.24 mmol) and piperidine (378 μL, 3.83 mmol) were added at room temperature, and the mixture was stirred at room temperature overnight. Subsequent to evaporation of the solvent, the residue was dissolved in ethyl acetate, and the organic layer was washed with water and brine, then dried over Na_2SO_4, and concentrated under reduced pressure. The residue was purified by silica gel column chromatography (ethyl acetate/hexane=1/4) to give ***Z*-8** (1.11 g, 70%) as a pale yellow solid. Pale yellow needles. Mp: 119–120 °C (CH_2Cl_2/hexane). ^{1}H NMR (CD_3CN) δ=8.20–8.17 (m, 2H), 7.46–7.37 (m, 3H), 6.96 (s, 1H), 3.66 (t, *J*=5 Hz, 2H), 2.80–2.76 (m, 2H), 1.85–1.74 (m, 4H), 1.69–1.63 (m, 2H) ppm ^{13}C NMR (CD_2Cl_2) δ=170.2, 168.6, 140.0, 134.9, 132.4, 130.2, 128.9, 126.6, 41.0, 32.0, 31.0, 29.4, 26.0 ppm. IR (KBr) ν_{max}: 1643, 1711 cm^{-1}. UV (CH_2Cl_2) λ_{max} nm (log ε): 293 (4.06), 358(4.32). MS (FAB) *m/z* 241 ($M+H^+$). Anal. Calcd for C 74.97, H 6.71, N 11.66; found C 74.90, H 6.75, N 11.62.

*4.3.4. (E)-2-Benzylidene-6,7,8,9-tetrahydro-2H-imidazo[1,2-a]azepin-3(5H)-one (**E-8**).* A solution of ***Z*-8** (400 mg, 1.67 mmol) in benzene (16 mL) was left under a UV light (365 nm, 16 W) at room temperature for 20 h. After evaporation of the solvent, the residue was purified by silica gel column chromatography (ethyl acetate/hexane=1/2 to 1/1) in a darkroom to give ***E*-8** (171 mg, 43%) and recovered ***Z*-8** (168 mg, 42%). Yellow needles. Mp: 125–126 °C. (CH_2Cl_2/hexane). ^{1}H NMR (CD_3CN) δ=8.27–8.23 (m, 2H), 7.46–7.40 (m, 3H), 7.21 (s, 1H), 3.67 (t, *J*=4 Hz, 2H), 2.71–2.66 (m, 2H), 1.84–1.70 (m, 4H), 1.69–1.62 (m, 2H) ppm ^{13}C NMR (CD_2Cl_2) δ=167.1, 165.3, 141.0, 136.4, 134.1, 131.8, 130.6, 128.6, 40.9, 31.7, 31.0, 29.4, 26.1 ppm. IR (KBr) ν_{max}: 1635, 1695 cm^{-1}. UV (CH_2Cl_2) λ_{max} nm (log ε): 289 (4.09), 359 (4.13). HRMS (FAB) Calcd for $C_{15}H_{17}N_2O$ ($M+H^+$): 241.1341. Found: 241.1339.

Acknowledgements

This work was supported by JSPS KAKENHI Grant Number 24790029.

Supplementary data

Supplementary data (Experimental procedures for the syntheses of **9** and **10**, copies of the ^{1}H NMR and ^{13}C NMR spectra for all new compounds, excitation–emission contour plots of crystalline powders **4**, **5a**, **5b** and **6** and supplementary figures for the molecular packing of the X-ray crystal structures. Supplementary data associated with this article can be found in the online version.) related to this article can be found at http://dx.doi.org/10.1016/j.tet.2015.05.073.

References and notes

1. Review Zimmer, M. *Chem. Rev.* **2002**, *102*, 759–781.
2. (a) Ormö, M.; Cubitt, A. B.; Kallio, K.; Gross, L. A.; Tsien, R. Y.; Remington, S. J. *Science* **1996**, *273*, 1392–1395; (b) Yang, F.; Moss, L. G.; Phillips, G. N., Jr. *Nat. Biotechnol.* **1996**, *14*, 1246–1251.
3. (a) Voliani, V.; Bizzarri, R.; Nifosì, R.; Abbruzzetti, S.; Grandi, E.; Viappiani, C.; Beltram, F. *J. Phys. Chem. B* **2008**, *112*, 10714–10722; (b) Yang, J.-S.; Huang, G.-J.; Liu, Y.-H.; Peng, S.-M. *Chem. Commun.* **2008**, 1344–1346.
4. A similar *Z*-*E* isomerization has been reported for benzylidene-oxazolone analogues: (a) Blanco-Lomas, M.; Campos, P. J.; Sampedro, D. *Org. Lett.* **2012**, *14*, 4334–4337; (b) Blanco-Lomas, M.; Funes-Ardoiz, I.; Campos, P. J.; Sampedro, D. *Eur. J. Org. Chem.* **2013**, 6611–6618; (c) Funes-Ardoiz, I.; Blanco-Lomas, M.; Campos, P. J.; Sampedro, D. *Tetrahedron* **2013**, *69*, 9766–9771.
5. Dong, J.; Abulwerdi, F.; Baldridge, A.; Kowalik, J.; Solntsev, K. M.; Tolbert, L. M. *J. Am. Chem. Soc.* **2008**, *130*, 14096–14098.
6. Some exceptions to such a 'dark' *E*-form are known: for example Petersen, J.; Wilmann, P. G.; Beddoe, T.; Oakley, A. J.; Devenish, R. J.; Prescott, M.; Rossjohn, J. *J. Biol. Chem.* **2003**, *278*, 44626–44631.
7. Examples of fluorescent GFP-chromophore analogues: (a) Kojima, S.; Ohkawa, H.; Hirano, T.; Maki, S.; Niwa, H.; Ohashi, M.; Inouye, S.; Tsuji, F. I. *Tetrahedron Lett.* **1998**, *39*, 5239–5242; (b) He, X.; Bell, A. F.; Tonge, P. J. *Org. Lett.* **2002**, *4*, 1523–1526; (c) Bourotte, M.; Schmitt, M.; Follenius-Wund, A.; Pigault, C.; Haiech, J.; Bourguignon, J.-J. *Tetrahedron Lett.* **2004**, *45*, 6343–6348; (d) Chen, K.-Y.; Cheng, Y.-M.; Lai, C.-H.; Hsu, C.-C.; Ho, M.-L.; Lee, G.-H.; Chou, P.-T. *J. Am. Chem. Soc.* **2007**, *129*, 4534–4535; (e) Stafforst, T.; Diederichsen, U. *Eur. J. Org. Chem.* **2007**, 899–911; (f) Huang, G.-J.; Yang, J.-S. *Chem.—Asian J.* **2010**, *5*, 2075–2085; (g) Kang, J.; Zhao, G.; Xu, J.; Yang, W. *Chem. Commun.* **2010**, 2868–2870; (h) Li, Y.; Shi, L.; Qin, L.-X.; Qu, L.-L.; Jing, C.; Lan, M.; James, T. D.; Long, Y.-T. *Chem. Commun.* **2011**, 4361–4363; (i) Katritzky, A. R.; Yoshioka-Tarver, M.; El-Gendy, B. E.-D. M.; Hall, C. D. *Tetrahedron Lett.* **2011**, *52*, 2224–2227; (j) Paige, J. S.; Wu, K. Y.; Jaffrey, S. R. *Science* **2011**, *333*, 642–646; (k) Wenge, U.; Wagenknecht, H.-A. *Synthesis* **2011**, 502–508; (l) Chuang, W.-T.; Hsieh, C.-C.; Lai, C.-H.; Lai, C.-H.; Shih, C.-W.; Chen, K.-Y.; Hung, W.-Y.; Hsu, Y.-H.; Chou, P.-T. *J. Org. Chem.* **2011**, *76*, 8189–8202; (m) Kang, J.; Fang, X.; Chen, X.; Zhao, G.; Ren, A.; Xu, J.; Yang, W. *Eur. J. Inorg. Chem.* **2011**, 5322–5327; (n) Cacciarini, M.; Nielsen, M. B.; de Castro, E. M.; Marinescu, L.; Bols, M. *Tetrehedron Lett.* **2012**, *53*, 973–976; (o) Huang, G.; Zhang, G.; Wu, Y.; Liao, Q.; Fu, H.; Zhang, D. *Asian J. Org. Chem.* **2012**, *1*, 352–358; (p) Shi, L.; Li, Y.; Liu, Z.-P.; James, T. D.; Long, Y.-T. *Talanta* **2012**, *100*, 401–404; (q) Huang, G.-J.; Ho, J.-H.; Prabhakar, C.; Liu, Y.-H.; Peng, S.-M.; Yang, J.-S. *Org. Lett.* **2012**, *14*, 5034–5037; (r) Tou, S.-L.; Huang, G.-J.; Chen, P.-C.; Chang, H.-T.; Tsai, J.-Y.; Yang, J.-S. *Chem. Commun.* **2014**, 620–622; (s) Baranov, M. S.; Solntsev, K. M.; Baleeva, N. S.; Mishin, A. S.; Lukyanov, S. A.; Lukyanov, K. A.; Yampolsky, I. V. *Chem.—Eur. J.* **2014**, *20*, 13234–13241; (t) very recent report Huang, G.-J.; Lin, C.-J.; Liu, Y.-H.; Peng, S.-M.; Yang, J.-S. *Photochem. Photobiol.* **2015**, *91*, 714–722.
8. Tolbert's group has reported a series of GFP-chromophore analogues: (a) Tolbert, L. M.; Baldridge, A.; Kowalik, J.; Solntsev, K. M. *Acc. Chem. Res.* **2012**, *45*, 171–181 and references therein; (b) Baranov, M. S.; Lukyanov, K. A.; Borissova, A. O.; Shamir, J.; Kosenkov, D.; Slipchenko, L. V.; Tolbert, L. M.; Yampolsky, I. V.; Solntsev, K. M. *J. Am. Chem. Soc.* **2012**, *134*, 6025–6032; (c) Fery-Forgues, S.; Veesler, S.; Fellows, W. B.; Tolbert, L. M.; Solntsev, K. M. *Langmuir* **2013**, *29*, 14718–14727; (d) Samanta, S. R.; Silva, J. P. D.; Baldridge, A.; Tolbert, L. M. *Org. Lett.* **2014**, *16*, 3304–3307.
9. Dong, J.; Solntsev, K. M.; Tolbert, L. M. *J. Am. Chem. Soc.* **2009**, *131*, 662–670.
10. Wu, L.; Burgess, K. *J. Am. Chem. Soc.* **2008**, *130*, 4089–4096.
11. A part of this work appeared as a preliminary letter Ikejiri, M.; Tsuchino, M.; Chihara, Y.; Yamaguchi, T.; Imanishi, T.; Obika, S.; Miyashita, K. *Org. Lett.* **2012**, *14*, 4406–4409.
12. Baldridge, A.; Kowalik, J.; Tolbert, L. M. *Synthesis* **2010**, 2424–2436.
13. (a) Gong, X.; Yang, H.; Liu, H.; Jiang, Y.; Zhao, Y.; Fu, H. *Org. Lett.* **2010**, *12*, 3128–3131; (b) Lee, C.-Y.; Chen, Y.-C.; Lin, H.-C.; Jhong, Y.; Chang, C.-W.; Tsai, C.-H.; Kao, C.-L.; Chien, T.-C. *Tetrahedron* **2012**, *68*, 5898–5907; (c) Baranov, M. S.; Solntsev, K. M.; Lukyanov, K. A.; Yampolsky, I. V. *Chem. Commun.* **2013**, 5778–5780; (d) Review Ivashkin, P. E.; Yampolsky, I. V.; Lukyanov, K. A. *Russ. J. Bioorg. Chem.* **2009**, *35*, 652–669.
14. The syntheses of glycinates **10e**–**h** were carried out by a partly modified O'Donnell method with corresponding imines and glycinate hydrochloride (Table S1 in supplementary data) O'Donnell, M. J.; Polt, R. L. *J. Org. Chem.* **1982**, *47*, 2663–2666.
15. Narayana Rao, M.; Holkar, A. G.; Ayyangar, N. R. *Tetrahedron Lett.* **1989**, *30*, 4717–4720.
16. Campagna, F.; Carotti, A.; Casini, G. *J. Heterocycl. Chem.* **1990**, *27*, 1973–1977.
17. Several BDI analogues are known to exhibit fluorescence in the solid state: see Ref. 7l,o,r,t and 9.
18. Second emissions of other DAINs were not so prominent. Contour plots for other typical DAINs are given as Supplementary data.
19. Review Shimizu, M.; Hiyama, T. *Chem.—Asian J.* **2010**, *5*, 1516–1531.
20. A similar dual emission was reported for a certain type of BDI analogue: see Ref. 9.
21. Niwa, H.; Inouye, S.; Hirano, T.; Matsuno, T.; Kojima, S.; Kubota, M.; Ohashi, M.; Tsuji, F. I. *Proc. Natl. Acad. Sci. U.S.A.* **1996**, *93*, 13617–13622 Ref. 7a.
22. Prescott, M.; Ling, M.; Beddoe, T.; Oakley, A. J.; Dove, S.; Hoegh-Guldberg, O.; Devenish, R. J.; Rossjohn, J. *Structure* **2003**, *11*, 275–284.
23. Review Feringa, B. L. *J. Org. Chem.* **2007**, *72*, 6635–6652. Since fluorenylidene and thioxanthenylidene moieties are typical components of the light-driven molecular motors, we consider that the double bond isomerization is a crucial factor for the fluorescence quenching of DAINs, especially for the 3rd-generation.
24. Grabowski, Z. R.; Rotkiewicz, K.; Rettig, W. *Chem. Rev.* **2003**, *103*, 3899–4031.
25. Review Hong, Y.; Lam, J. W. Y.; Tang, B. Z. *Chem. Soc. Rev.* **2011**, *40*, 5361–5388.
26. CCDC-1034530–1034533 contain the supplementary crystallographic data for this paper. 1034530(1), 1034531 (3a), 1034532 (5d), 1034533 (6). These data can be obtained free of charge from The Cambridge Crystallographic Data Centre via www.ccdc.cam.ac.uk/data_request/cif.
27. Bhattacharjya, G.; Savitha, G.; Ramanathan, G. *J. Mol. Struct.* **2005**, *752*, 98–103.
28. A certain type of BDI analogue has been reported to accompany a photoreaction such as double bond isomerization and [2+2] photo-dimerisation in the solid state Naumov, P.; Kowalik, J.; Solntsev, K. M.; Baldridge, A.; Moon, J.-S.; Kranz, C.; Tolbert, L. M. *J. Am. Chem. Soc.* **2010**, *132*, 5845–5857; for a oxazolone analogue: Runčevski, T.; Blanco-Lomas, M.; Marazzi, M.; Cejuela, M.; Sampedro, D.; Dinnebier, R. E. *Angew. Chem. Int. Ed.* **2014**, *53*, 6738–6742.
29. A similar quenching caused by intermolecular π-overlap within dimers was reported for some BDI analogues containing a large aromatic ring: see Ref. 7o.
30. A similar relationship between spacing and fluorescence wavelength was reported for a bis(phenylethynyl)benzene derivative Thomas, R.; Varghese, S.; Kulkarni, G. U. *J. Mater. Chem.* **2009**, *19*, 4401–4406.